Quenching and Partitioning of Plate Steel: Thermal Gradients and Microstructure Development During Quenching

This work explores the applicability of the quenching and partitioning (Q&P) process to plate steel, considering through-thickness thermal profiles and associated microstructural gradients for different plate thicknesses. A one-dimensional numerical model was used to simulate temperature evolution in a flat plate. Simulated cooling and heating media were selected to represent a wide range of potential industrial processes. Through-thickness microstructures associated with the 1D thermal gradients are considered in the context of alloying and Q&P process design.

Authors

R.A. Stewart
M.S. student, Colorado School of Mines, Golden, Colo., USA
rachaelstewart@mines.edu

J.G. Speer
professor, George S. Answell Department of Metallurgical and Materials Engineering, Colorado School of Mines, Golden, Colo., USA
jspeer@mines.edu

B.G. Thomas
professor, Mechanical Engineering Department, Colorado School of Mines, Golden, Colo., USA
bgthomas@mines.edu

A.J. Clarke
associate professor, George S. Ansell Department of Metallurgical and Materials Engineering, Colorado School of Mines, Golden, Colo., USA
amyclarke@mines.edu

E. De Moor
assistant professor, Advanced Steel Processing and Products Research Center, George S. Ansell Department of Metallurgical and Materials Engineering, Colorado School of Mines, Golden, Colo., USA
edemoor@mines.edu

The third generation of advanced high-strength steels (AHSS) is a class of sheet steels characterized by mixed microstructures containing retained austenite (RA).[1] Such microstructures provide excellent combinations of strength, ductility, formability and toughness, which are of interest to the automotive industry.[2] Such microstructures have also shown promise in wear applications.[3,4] Quenching and partitioning (Q&P) proposed by Speer et al.[5] has been commercialized as a heat treatment for low-alloy sheet steels, to produce third-generation AHSS microstructures and properties.

The Q&P process, shown in the processing schematic in Fig. 1, has two steps. An initial quenching process, designed to reach a specific initial quenching temperature where a desired martensitic fraction is formed, and a partitioning process designed to allow a substantial portion of the carbon in the martensite to diffuse into the austenite, while minimizing loss of carbon to cementite or transition carbide precipitation. The increased carbon stabilizes the retained austenite, which in turn provides increased ductility and toughness to the final microstructure. A final quench to room temperature completes the process. These precise microstructural processes and targets place stringent demands on process control during both steps. Q&P literature based on sheet processing cites the quench temperature (QT), partitioning temperature (PT) and partitioning time (Pt) as important parameters that should be carefully controlled.[5,6]

Reaching the desired QT is critical to martensite formation during the quenching step, and balancing the subsequent partitioning times and temperatures is critical to maximize retained austenite contents. The optimum QT is defined as the temperature at which RA, after idealized (full) partitioning, will have a martensite start temperature (M_s) below room temperature, thus minimizing or precluding the formation

Figure 1

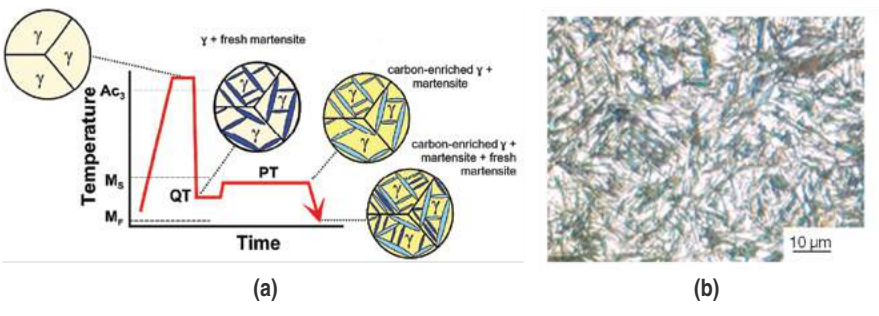

Schematic of two-step quenching and partitioning (Q&P) sheet thermal processing, with full austenitization. Quench temperature (QT) and partitioning temperature (PT) are quenching and partitioning temperatures, respectively. M_s and M_f are the martensite start and finish temperatures. Expected microstructures at each step are illustrated[7] (a). Light optical micrograph of 9260 Q&P: 190–400°C-10 s, tint etched using picral, then sodium metabisulfite, retained austenite (white) and partitioned martensite (dark)[8] (b).

of fresh martensite on final cooling.[5] The optimum QT can be estimated by application of the Koistinen and Marburger (K-M) equation (Eq. 1), where V_m is volume of martensite, K is a constant with a typical value of 0.011 and M_s is the martensite start temperature, which can be estimated according to empirical functions, such as Eq. 2, proposed by Andrews,[9] or measured directly, using dilatometry.

$$V_m = 1 - e^{-K(M_s - QT)} \quad \text{(Eq. 1)}$$

$$M_s = 539 - 423C - 30.4Mn - 17.7Ni - 12.1Cr - 7.5Mo \quad \text{(Eq. 2)}$$

For a given quench temperature, if full partitioning is assumed to take place, the carbon content of the retained austenite can be estimated using the lever rule. The Ms of the untransformed austenite is recalculated (Eq. 2) taking into account the updated carbon content. Eq. 1 is again used to estimate the fraction of austenite that transforms to martensite upon final cooling to room temperature. Using this methodology, the fraction of partitioned martensite, untransformed austenite and "fresh" martensite can all be estimated in the final microstructure.

Fig. 2 illustrates the estimated retained austenite fraction after partitioning and cooling to room temperature versus the QT prior to partitioning for a 0.2C (wt.%) steel with a M_s temperature of 400°C. For this steel, the optimum QT is 250°C, which corresponds to a retained austenite content of 19 vol.%.

Figure 2

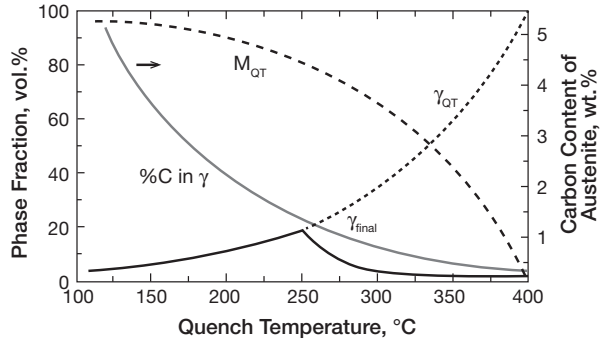

Calculated phase fractions as a function of initial quench temperature in a hypothetical Q&P process with full partitioning. Phase fractions calculated for a 0.2C steel with M_s = 400°C. M_{QT} and γ_{QT} correspond to the amount of martensite and austenite present after quenching to QT. γ_{final} predicts the final austenite phase amount at room temperature. Wt.% carbon in the retained γ after idealized partitioning is indicated on the secondary axis.

It should be noted that the application of Eq. 1 assumes compositional and microstructural homogeneity following an interrupted quench step and a reheating step. The maximum estimated retained austenite has rarely been attained in previous Q&P experiments, likely due to competition from reactions such as carbide precipitation.[10,11] In addition, the maximum experimentally achieved retained austenite has not always corresponded to the estimated optimum QT for that partitioning treatment.[9]

This QT selection methodology is widely used[12–15] to select a range of QT for experimental work. A range of PT and Pt have also been used in experimental Q&P studies and a variety of Q&P microstructures have been produced; the amounts, morphology and distribution of phases change with alloying and processing.[6,10,16] Experimental Q&P studies have explored one-step[8,17,18] and two-step[6,7,11] processes through Gleeble simulation or dilatometry, as well as laboratory production of hot- and cold-rolled Q&P sheet.[16,19,20] A study by Thomas[21] developed the concept for Q&P hot-rolled sheet production, using coil cooling as the partitioning step. Thomas et al. noted the challenge in controlling the variability of microstructure and properties across the width and length of steel sheets that arise during coil cooling,[21] due to cooling rate variations.

The Q&P process has been commercialized for sheet steels, where thermal gradients through the thickness are small. A handful of studies have considered the possibility of applying Q&P in steel plate.[22–24] Hong et al. obtained Q&P microstructures with interesting properties in laboratory heat-treated plate, thus suggesting the opportunity for thick-plate Q&P.[22] Zhou et al. examined temperature and microstructural gradients in hot-rolled plate through thermal modeling and experimental validation.[23] The simulated thermal profiles predicted an inhomogeneous microstructure through a 20-mm-thick steel sample after a quench-partition-temper (Q-P-T) process (austenitizing for 3,600 seconds, quenching for 15 seconds then tempering by air cooling for 1,800 seconds). Experimental results confirmed this prediction: a "sandwich" microstructure was reported with lath martensite at the plate surfaces/subsurface and a mixture of lath martensite and bainite in the center where the steel cooled more slowly. This inhomogeneity in microstructure in the 20-mm-thick sample was neither predicted nor experimentally observed in a 12-mm-thick sample, which showed almost the same microstructures (martensite laths) throughout the cross-section.

The above studies suggest that microstructural variations may arise through the thickness in Q&P processing of plates, due to variation in cooling rates and thermal gradients. Unlike sheet Q&P processing, thermal gradients are important to consider in

Q&P processing of thick plate. In plate Q&P, these parameters are less defined; a range of QT-PT-Pts and therefore a range of microstructures will exist through the thickness. Control of microstructure and properties in Q&P plate therefore requires an understanding of the evolving thermal gradients. The influence of varying through thickness thermal histories on the Q&P process has not been systematically studied with the goal of commercially producing Q&P microstructures in thick plate. Thermal gradients induced during processing change with time, plate thickness and process parameters, and are therefore difficult to predict or measure experimentally for the wide range of thicknesses and processes of interest. This situation presents an important opportunity for a thermal model to be developed and applied as a tool to explore the effects of plate thickness, quench and reheat mediums on temperature profiles, and thus expected microstructure development.

This work focuses on the development and application of a thermal model to investigate thermal gradients induced during plate Q&P processing. The cooling profiles produced under various thicknesses and process conditions are simulated and the effects of thermal gradients on final microstructures are investigated. Final phase fractions are estimated by applying methods developed in sheet Q&P to the simulated plate thermal profiles.

Thermal Modeling Tool

Model Formulation — A simple finite-difference model was developed to simulate temperature evolution during the cooling of a flat steel plate. For a typical flat plate shown in Fig. 3a, where the thickness is small compared to plate length and width, the steepest temperature gradients are expected to develop through the thickness.

Transient heat conduction through a solid flat plate is described by Fourier's transient-conduction equation. The solutions to this partial differential equation provide the variation of temperature with both time and position in the plate. In the absence of internal heat generation, and assuming constant thermal properties, Fourier's equation is:

$$\frac{dT}{dt} = \alpha \frac{d^2x}{dt^2} + \frac{d^2y}{dt^2} + \frac{d^2z}{dt^2} \qquad \text{(Eq. 3)}$$

where
T = temperature,
t = time,
x, y and z = distances in the thickness, width and length directions, respectively, and
α = thermal diffusivity, defined as:

$$\alpha = \frac{k}{\rho C_p} \qquad \text{(Eq. 4)}$$

where
k = conductivity,
ρ = density and
C_p = specific heat.

The imposed boundary conditions for the cooling of the plate were forced convection with the convection coefficient, h, at the top and bottom plate surfaces. Assuming identical boundary conditions at the plate top and bottom surfaces creates a symmetry plane at the plate center, as shown in Fig. 3a. Ignoring variations near the plate ends and sides due to edge cooling, and assuming uniform heat transfer to the surface, this transient conduction problem simplifies to a single dimension, given by Eq. 5, and can be solved either analytically or numerically.

$$\frac{dT}{dt} = \alpha \frac{d^2x}{dt^2} \qquad \text{(Eq. 5)}$$

The finite-difference model solution to Eq. 5 can be approximated numerically as Eq. 6, by discretizing the domain into cells with nodes as shown in Fig. 3b, and performing an energy balance around each cell.

$$\frac{\Delta T}{\Delta t} = \frac{T_i^{t+1} - T_i}{\Delta t} \qquad \text{(Eq. 6)}$$

The notation in Eq. 6 includes a temperature term with indices for position and time: $T_{position(x)}^{time(n)}$

Expressions for temperature were obtained for each cell (Eqs. 7–9). The surface cell, where the convection boundary condition is applied, is "cell n;" the center cell, where the insulated boundary condition is applied, is "cell 1;" and the other cells comprising the interior are "cell i." The number of nodes (n = 50 nodes) was established based on a mesh size study.

$$T_1^{t+1} = T_1^t + \frac{2k\Delta t}{\rho C_p \Delta x^2}\left[T_2^t - T_1^t\right] \qquad \text{(Eq. 7)}$$

Figure 3

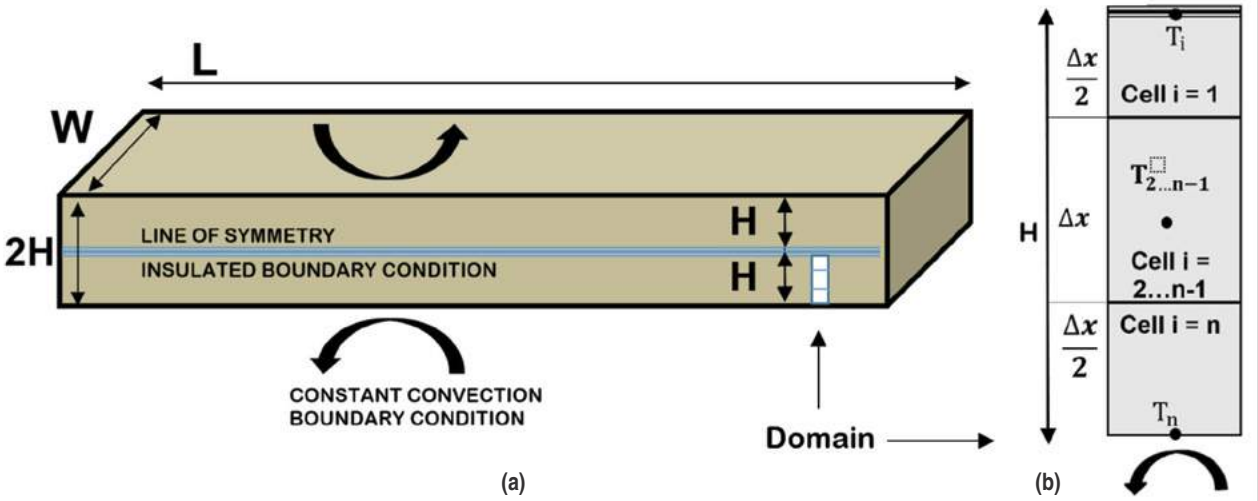

Flat plate geometry where thickness, 2H, is much less than the length, L, and width, W (a). Symmetric boundary conditions of constant convection at plate surfaces are illustrated with curved arrows. Modeled domain is a 1D slice of half the plate thickness. Close-up of the discretized domain showing cells, nodes and dimensions (b).

$$T_i^{t+1} = T_i^t + \frac{k\Delta t}{\rho C_p \Delta x^2}\left[T_{i-1}^t - 2T_i^t + T_{i+1}^t\right] \quad \text{(Eq. 8)}$$

$$T_n^{t+1} = T_i^t + \frac{2k\Delta t}{\rho C_p \Delta x^2}\left[T_{n-1}^t - T_n^t\right] + \frac{2h\Delta t}{\rho C_p \Delta x}\left[T_\infty - T_n^t\right] \quad \text{(Eq. 9)}$$

A transformed version of Eqs. 7–9 was written in MATLAB (Eqs. 10–12), and solved using the built-in MATLAB ordinary differential solver (ODE45) which uses a Runge-Kutta fourth-order approximation.

$$\frac{dT}{dt}_1 = \frac{2k}{\rho C_p dx^2}\left(T_2 - T_1\right) \quad \text{(Eq. 10)}$$

$$\frac{dT}{dt_i} = \frac{k}{\rho C_p dx^2}\left(T_{i-1} - 2T_i + T_{i+1}\right) \quad \text{(Eq. 11)}$$

$$\frac{dT}{dt_n} = \frac{2k}{\rho C_p dx^2}\left(T_{n-1} - T_n\right) + \frac{2h}{\rho C_p dx}\left(T_\infty - T_n\right) \quad \text{(Eq. 12)}$$

This numerical model was validated against an analytical model built in Microsoft Excel®, using a 20-term series[25] to solve a simple problem of transient quenching of a 24-mm-thick plate. The numerical model matched the analytical model within 0.001% maximum error at any of the 50 nodes, which verifies the numerical method.

The model was then applied to investigate a wide range of quenching scenarios and plate thicknesses, assuming constant steel properties (invariant with both temperature and microstructure), given in Table 1. A constant convection coefficient (that included radiation) and constant quench medium temperature selected from literature was adopted to represent each of three quenching processes. The latent heat of phase transformation was neglected for this simple study. In reality, quenching is a complex heat transfer process controlled by sample geometry, quench medium, agitation, fluid properties and workpiece thermal properties.[26,27] The convection coefficient is known to vary during quenching according to the vapor blanket, boiling and convective stages. Furthermore, the thermal properties, including density, conductivity and specific heat, are known to vary with microstructural phase, composition and temperature. Thus, the current study represents a first approximation to the real quenching processes.

Table 1

Parameters Used in the Simulated Cooling Scenarios

Parameter	Value	Reference
Thickness, 2H	50 mm; 18 mm; 6 mm	
Modeled half thickness, H	25 mm; 9 mm; 3 mm	
Initial temperature T_{ini}	1,100°C	
Quench bath temperature, T_{inf}	50°C	
Thermal conductivity, k	30 W/m – °K	30
Thermal diffusivity α	7.003 x 10^{-6} m^2/second	30
Specific heat C_p	560 J/kg – °K	30
Density, ρ	7650 kg/m^3	30
Quench convection coefficient, h	100 W/m^2 – °K; 1,000 W/m^2 – °K; 10,000 W/m^2 – °K	28
Quench fluid velocity/flowrate	40 m/second; 13 L/m^2 – s; 847 L/m^2 – s	29
Number of nodes	50	

Thermal Modeling Case Studies

— To investigate the first step of the Q&P process, the temperatures and thermal gradients produced under various quenching scenarios were examined through nine modeling case studies. Three plate thicknesses (6, 18 and 50 mm) were each simulated for three different quenching processes, starting from an initial temperature above A_{c3}, of 1,100°C. The three cooling processes of air cool, water spray quench and severe water quench were chosen to represent a wide

Figure 4

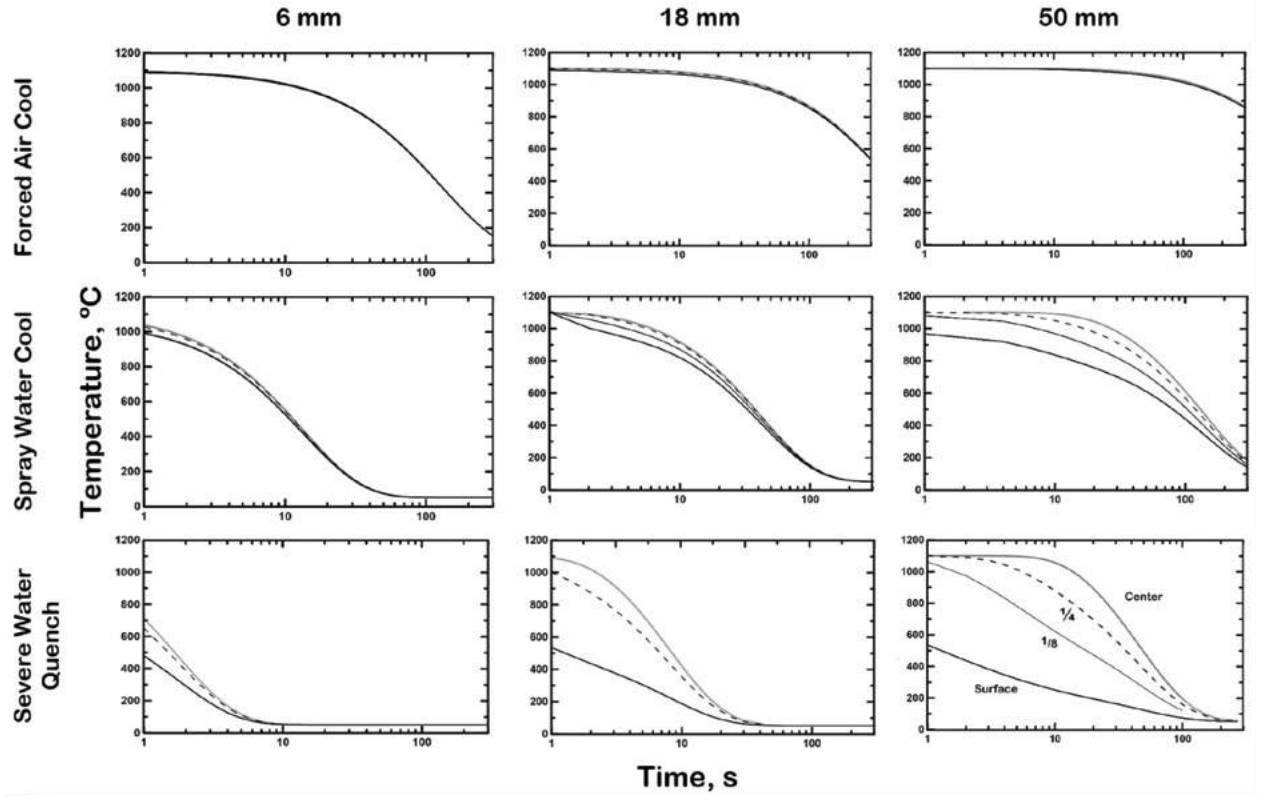

Thermal profiles for plate thicknesses 6, 18 and 50 mm quenched from 1,100°C using three quenching media: severe water quench (convection coefficient, h = 10,000 W/m^2 – °K), spray water cool (h = 1,000 W/m^2 – °K) and air cool (h = 100 W/m^2 – °K). Time is shown on log scale from 1 to 300 seconds. Thermal profiles at plate center are indicated with a gray line; quarter thickness position by a dashed line; one-eighth thickness position by a thin line and surface by a thick line.

range of potential process scenarios.[28] Approximate convection coefficients appropriate for each cooling process were selected from literature.[29,30] The value chosen for air cooling includes some forced convection, so the internal thermal gradients, cooling rate and temperature variations for natural convection cooling would be even smaller than the results shown here. Cooling media temperatures were fixed at 50°C. Process parameters and material properties used in the simulations are shown in Table 1.

Results and Discussion

Thermal Model Results — Results of the nine cooling scenarios are presented as temperature-time plots in Fig. 4. The thermal histories at three positions through the thickness are shown for the 6-mm and 18-mm plates: center, surface and quarter point. Four locations are shown for the 50-mm plate: center, surface, quarter point and eighth point. Thermal histories are shown for quench times up to 300 seconds, or 5 minutes. Note that the temperature change with respect to distance is referred to as the thermal gradient and the temperature change with respect to time is referred to as the cooling rate.

Comparing the temperature-time thermal profiles in Fig. 4 from left to right, the effect of thickness on thermal gradients and cooling rates can be examined. Comparing the profiles from top to bottom, the effect of quenching medium on the thermal gradients and cooling rates in a plate can be examined.

The cooling rate (°C/second) at a given time and position in a given plate is the slope of the temperature history shown in Fig. 4. At early quenching times, the plate surfaces cool much more rapidly than the plate centers. However, at longer times, the surface cooling rates may be exceeded by center cooling rates. The rapid surface cooling at early times is driven by the difference in temperature between the plate surface and the cooling media (the ΔT term in Eq. 6); a larger difference in temperature will cause more rapid heat extraction. At longer quench times, the conductive heat transfer from plate center to plate surface exceeds the convective heat transfer from plate surface to quench media, so the interior cools faster.

The extent of the difference between surface and center cooling rates depends greatly on thickness and quench severity. Under air cooling, heat extraction at the plate surfaces is slow, and the plate cools at a near-uniform rate through the thickness. Air cooling in the 6-mm, 18-mm and even 50-mm plates is uniform from surface to center, as illustrated by the overlapping thermal histories. Quench severity greatly increases the surface cooling rates in all plate thicknesses, as expected, but quench severity does not increase the center cooling rates in all thicknesses. In the case of the 6-mm plate, the center cooling rate increases by an order of magnitude with increasing quench severity. In contrast, the cooling rate at the center of the thicker plates varies very little between quenching processes, as the center is insulated from the convection applied at the surface. Consequently, steep thermal gradients develop during spray water cooling and severe water quenching of the thick plates. The surface and near-surface lose heat very rapidly, while the plate center retains heat for longer times. As illustrated in Fig. 4, the center of the severely quenched 50-mm plate remains at the initial temperature of 1,100°C for 10 seconds. In summary, through-thickness variations in temperature, temperature gradient and cooling rate all increase with increasing plate thickness, and with increasing quench severity.

Application of Cooling Profiles to Q&P Processing Response — In the context of the Q&P process, the cooling rates during initial quenching are important because they control any diffusional phase transformations during quenching, which would reduce the extent of martensite formation. The temperature gradients after initial quenching are important, because the lowest temperature reached at the end of the quench step largely controls the initial martensite phase fraction, which, in turn, influences the final phase fractions. To generate classic Q&P microstructures, the quench step must meet two important criteria. First, the cooling rate at every position through the thickness should be sufficient to avoid intermediate diffusional transformation products, such as ferrite and cementite in pearlite or bainite. Second, the temperature at every position through the thickness after quenching should form a controlled amount of martensite to allow austenite stabilization during partitioning.

The criteria for cooling rate will be examined first. Then, the effects of thermal gradients on Q&P microstructures will be examined in some depth. Thermal gradients present a difficult microstructural challenge, and have not been previously considered in the context of Q&P.

Importance of Cooling Rates During the Initial Quench Step of Q&P Response — Ideally, the cooling rate at every position through the plate thickness should be sufficient to form only martensite during quenching. Critical cooling rates, often reported in the range of temperatures between 800 and 500°C, are alloy specific. Linear approximations of the cooling rates between 800 and 500°C and the corresponding times to reach an M_s temperature of 400°C are presented in Table 2 for each of the nine cases. These results should be helpful in selecting alloys with sufficient hardenability for any desired cooling condition.

Table 2

Average Cooling Rates From 800 °C to 500 °C at Center and Surface for Each Quench Process and Plate Thickness

Plate thickness	Cooling medium	Center °C/second	Surface °C/second	Time for plate center to reach M_s 400°C (minute:second)
50 mm	Severe water quench	13	155	1:00
	Water spray quench	4	4	2:55
	Air cool	0.5	0.5	20:02
18 mm	Severe water quench	72	273	0:10
	Water spray quench	14	14	0:48
	Air cool	1.6	1.6	7:09
6 mm	Severe water quench	347	386	0:02
	Water spray quench	44	45	0:14
	Air cool	5	5	2:21

Figure 5

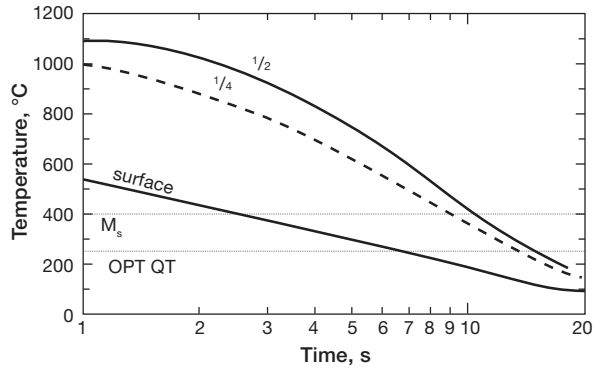

Simulated thermal history for severely water-quenched 18-mm plate from 1,100°C for 20 seconds. M_s (400°C) and optimum QT (~250°C) indicated for a 0.2 wt.% C steel.

Analyzing the cooling behaviors in Fig. 4 with respect to Q&P processing, certain thicknesses may be more suitable than others for the different cooling processes. For example, air cooling may be impractical for thicknesses above 6 mm as cooling rates (less than 2°C/second) may be too slow to form martensite and highly hardenable alloys would be required for thicker sections under air cooling conditions.

Spray water quenching and severe water quenching achieve shorter cooling times in the thicker sections (under 3 minutes), although both introduce thermal gradients. Thermal gradients naturally increase with quench severity and thickness. Severe water quenching produces very steep thermal gradients: up to 700°C variation in through-thickness temperature in thick plate. Spray cooling shows promise for a controlled quench rate across a range of thicknesses where the cooling times are reasonable and thermal gradients are more modest.

Thermal Gradient Effects on Through-Thickness Microstructural Variation

— The effect of thermal gradients on the expected phase distribution after quenching was estimated from the thermal model results using the Koistinen and Marburger equation (Eq. 1). The thermal histories in the 18-mm plate during the first 20 seconds of severe water quenching are shown as an example. The thermal histories at the center, quarter point and surface positions are enlarged in Fig. 5 for this example.

Examining the thermal histories shown in Fig. 5, in the context of the transformation behavior for an alloy with an assumed M_s of 400°C, the plate surface reaches an M_s of 400°C in ~2–3 seconds, while the plate center does not reach M_s until 10 seconds. Thus, the phase distributions change rapidly during the first 20 seconds of severe water quenching of this 0.2 wt.% C steel. Assuming full partitioning, phase fractions after partitioning and final cooling to room temperature can also be estimated. The estimated phase distributions after initial quenching and final cooling are illustrated in Fig. 6. Fig. 6 shows the phase fractions as a function of temperature at each position through the thickness, from surface to center, after quenching for five different times: 6, 8, 10, 15 and 20 seconds. Fractions of martensite and untransformed austenite are shown as a function of QT in the left column of Fig. 6; final phase distributions after cooling to room temperature are shown on the right, including the fractions of retained austenite and fresh martensite.

Fig. 6 shows the phase distributions estimated in the 18-mm plate after quenching for 6 seconds: a small region at the plate surface has transformed to 75 vol.% martensite, while the remainder of the plate is fully austenitic. After 8 seconds, the plate surface has transformed to 80% martensite while the plate center has not reached M_s. After 10 seconds, the plate surface has just reached M_s so that the microstructural gradient ranges from 0 vol.% martensite at the center, to greater than 90% at the surface. After 15 seconds and 20 seconds, the complete plate thickness from center to surface, contains above 75 vol.% martensite and 85 vol.% martensite, respectively.

The estimated final phase distributions, shown in the right-hand column in Fig. 6, also vary considerably with quench time. After a 6-second quench, an

Figure 6

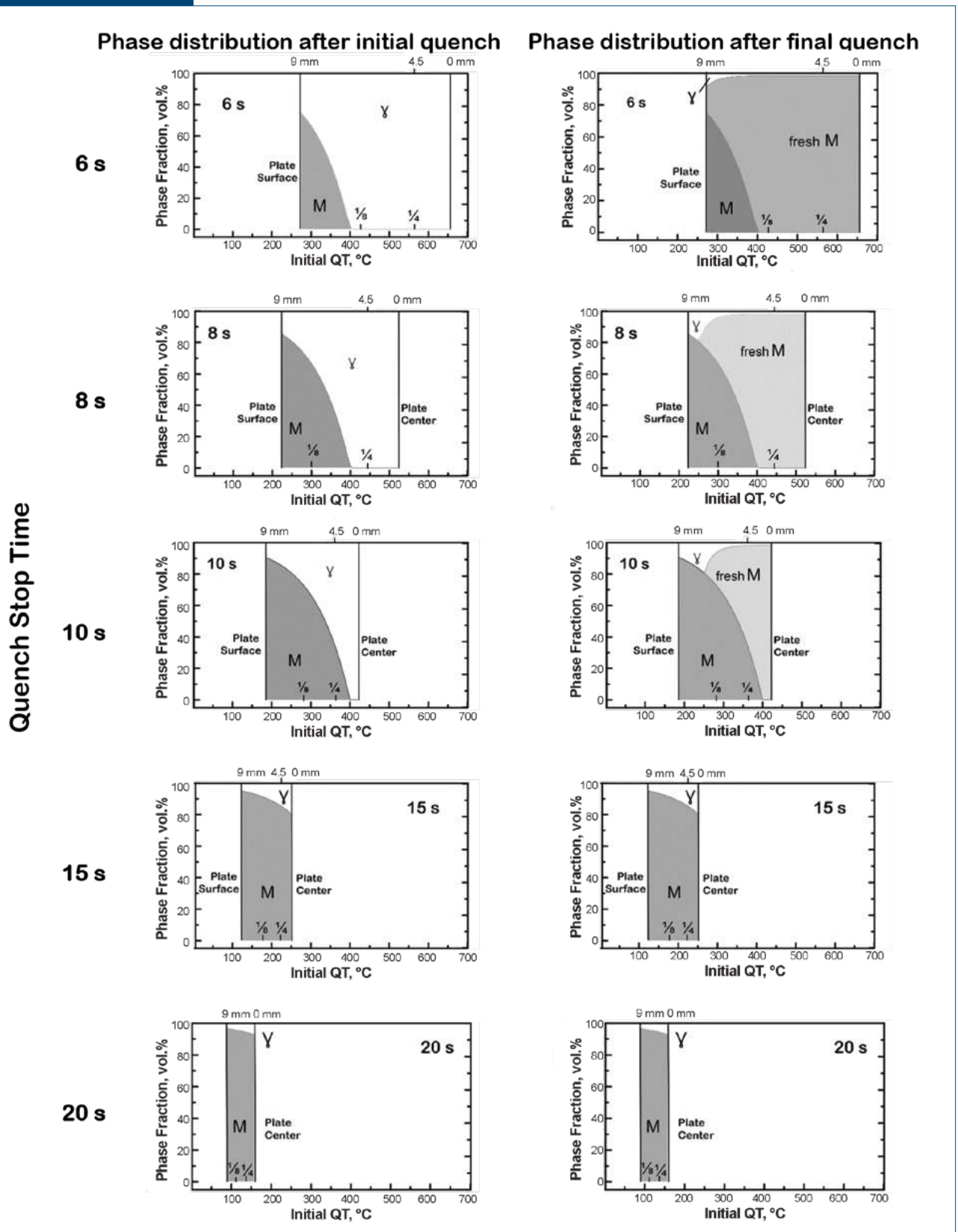

Estimated phase fractions through the thickness of an 18-mm plate severe water-quenched from 1,100°C as a function of initial quench temperature, after quenching for 6, 8, 10, 15 and 20 seconds. Estimated final phase fractions after cooling to room temperature (assuming full partitioning) as a function of initial quench temperature, for initial quench times of 6, 8, 10, 15 and 20 seconds. Phase fractions are shown for a 0.2 wt.% C alloy with an M_s of 400°C. Martensite indicated with M, austenite indicated with γ and martensite formed during final cooling indicated with fresh M.

idealized partitioning treatment and a final quench to room temperature, the plate is completely martensitic, except for a small fraction of retained austenite (7 vol.%) at a depth of 0.1 mm below the plate surface. For an idealized partitioning treatment after an 8-second initial quench, the microstructure from plate surface to 1 mm in depth contains appreciable amounts of retained austenite: 15 vol.% at the surface, increasing to 19 vol.% at a depth of 0.4 mm beneath the surface, then decreasing to 5 vol.% at a depth of 1 mm. The remaining thickness of the plate contains less than 2 vol.% retained austenite. After an initial 10-second quench, up to a fifth of the plate (within approximately 2 mm of the surface) contains greater than 10 wt.% retained austenite. A quench time of 15 seconds corresponds to the time at which the plate center reaches the optimum QT, so that no new martensite is formed at any location through the thickness on final cooling. A quench time of 15 seconds represents an important time for a severe water quench of this alloy: the maximum possible distribution (i.e., integrated over the cross-section) of austenite is stabilized to room temperature during ideal partitioning. The retained austenite content varies from 1.2 vol.% at the plate surface to 19 vol.% at the plate center for this condition. After a 20-second quench time, no fresh martensite is formed on final cooling as every location through the thickness is below the optimum QT; however, the corresponding austenite distribution does not reach the maximum of 19 vol.% at any location through the cross-section. The plate center contains 7 vol.% retained austenite; the plate surface contains 3 vol.% retained austenite.

This illustration of phase distribution variations due to thermal gradients shows the importance of the quenching step in controlling the amount of austenite that can be stabilized during partitioning. The maximum austenite content is retained at the location where the temperature corresponds to the optimum QT, which can be controlled with quench stop time. The quench stop time is therefore an important processing parameter and must be tailored to the selected alloy. A variety of quench stop time selection methods could be considered. This time could be selected to achieve a desired final phase distribution, or a specified phase fraction at a desired location through the thickness. However, controlling the phase fractions by keeping this time within a few seconds will require stringent process control. Nonetheless, the methodology presented here helps to predict the response to processing, and thus enables process design.

It is important to acknowledge that this analysis has assumed idealized partitioning. Heating profiles also need to be considered to incorporate the partitioning aspect of Q&P processing in a more substantial way. Partitioning of sheet steel is commonly conducted during a one-step hold, typically for short times (400°C for 10 seconds is a common sheet partitioning treatment). Reheating of plate could perhaps be achieved through furnace reheating or induction heating. Induction heating after cooling is not commonly applied to plate production, but literature suggests that such a configuration has been used for tempering in one facility.[31] As Q&P plate process design efforts continue, the influence of heating characteristics and thermal gradients will be further examined. The analysis provided here, focused on the initial cooling behavior, should already be quite helpful in Q&P process design, as it provides an estimate of the through-thickness distribution of phases in the final product, under idealized partitioning kinetics.

Conclusions

While past research in quenching and partitioning (Q&P) has mostly focused on sheet steels, the range of cooling rates and thermal gradients that develop in thick sections during processing present a new challenge in obtaining Q&P microstructures. Understanding the thermal history at each location through the thickness is essential to controlling microstructural variations. A thermal modeling tool was developed to study the cooling histories at each location during the quenching of different plate thicknesses with different quench process severities. The results were evaluated by adapting concepts from sheet Q&P to estimate the initial and final martensite phase fractions for a 0.2 wt.% C steel with an M_s temperature of 400°C. For the design of the quench step, nine case studies were presented, examining three plate thicknesses under three cooling media. Air cooling produces uniform temperature distributions, and thus microstructures, although it may be impractical given the long times to reach typical Q&P QTs. Spray cooling shows promise for a controlled quench across a range of thicknesses where the cooling times are reasonable and thermal gradients are modest. Severe water quenching produces severe thermal gradients in the thicker plates. Microstructural variations through the thickness were estimated assuming idealized partitioning, so as to quantify thermal gradient effects on initial and final phase fractions. Quench stop time is an important parameter to select and control, in order to influence the final microstructure, according to the methodology developed here. This work will continue in the future to incorporate industrial heating methods to investigate the partitioning step of Q&P process design.

Acknowledgments

The authors gratefully acknowledge the Advanced Steel Processing and Products Research Center sponsors for their support of this work.

References

1. D.K. Matlock and J.G. Speer, "Processing Opportunities for New Advanced High-Strength Sheet Steels," *Materials and Manufacturing Processes,* Vol. 25, Nos. 1–3, 2010, pp. 7–13.
2. L. Wang and W. Feng, "Development and Application of Q&P Sheet Steels," *The Recent Scenario in Steel Science and Technology,* 2011, pp. 67–73.
3. T. Liu, M.T. Kiser and T.E. Clements, "Effect of Microstructures on Low-Stress Abrasive Wear of Steel Plates," *International Symposium on the Recent Developments in Plate Steels,* 2011, pp. 71–80.
4. P. Wolfram, "The Microstructural Dependence of Wear Resistance in Austenite Containing Plate Steels," M.S. thesis, Colorado School of Mines, 2013.
5. J. Speer, D.K. Matlock, B.C. De Cooman and J.G. Schroth, "Carbon Partitioning Into Austenite After Martensite Transformation," *Acta Materialia,* Vol. 51, No. 9, 2003, pp. 2611–2622.
6. A.J. Clarke, "Carbon Partitioning Into Austenite From Martensite in a Silicon-Containing High-Strength Sheet Steel," Ph.D. thesis, Colorado School of Mines, 2006.
7. D.K. Matlock, V.E. Brautigam and J.G. Speer, "Application of the Quenching and Partitioning (Q&P) Process to a Medium-Carbon, High-Si Microalloyed Bar Steel," *Materials Science Forum,* Vol. 426–432, No. 2003, 1662–9752, pp. 1089–1094.
8. F.L.H. Gerdemann, J.G. Speer and D.K. Matlock, "Microstructure and Hardness of Steel Grade 9260 Heat-Treated by the Quenching and Partitioning (Q&P) Process," *MS&T Conference Proceedings,* 2004, pp. 439–449.
9. T. Nyyssonen and C.J. Van Tyne, unpublished research, Colorado School of Mines, 2016.
10. J.G. Speer, E. De Moor and A.J. Clarke, "Critical Assessment 7: Quenching and Partitioning," *MS&T Conference Proceedings,* Vol. 31, No. 1, 2015, pp. 3–9.
11. D.T. Pierce, D.L. Coughlin, K.D. Williamson, A.J. Clarke, J.G. Speer, D.K. Matlock and E. De Moor, "Mossbauer Spectroscopy Investigation of Transition Carbides in Quenched and Partitioned Steel," *Proceedings of the International Conference on Solid-Solid Phase Transformations in Inorganic Materials,* Vol. 8, 2015, pp. 91–98.
12. A.L. de Araújo, "Effects of Microalloying on Hot-Rolled and Cold-Rolled Q&P Steels," M.S. thesis, Colorado School of Mines, 2016.
13. J. Kahkonen, "Quenching and Partitioning Response of Carbon-Manganese-Silicon Sheet Steels Containing Nickel, Molybdenum, Aluminum and Copper," M.S. thesis, Colorado School of Mines, 2016.
14. M.J. Santofimia, L. Zhao and J. Sietsma, "Overview of Mechanisms Involved during the Quenching and Partitioning Process in Steels," *Metallurgical and Materials Transactions A: Physical Metallurgy and Materials Science,* Vol. 42, No. 12, 2011, pp. 3620–3626.
15. D. De Knijf, E.P. Da Silva, C. Föjer and R. Petrov, "Study of Heat Treatment Parameters and Kinetics of Quenching and Partitioning Cycles," *Materials Science and Technology,* Vol. 31, 2015, pp. 817–828.
16. J.G. Speer, A.L. Araujo, D.K. Matlock and E. De Moor, "Nb-Microalloying in Next-Generation Flat-Rolled Steels: An Overview," *Materials Science Forum,* Vol. 879, No. 1662–9752, 2017, pp. 1834–1840.
17. X. Tan, Y. Xu, X. Yang and D. Wu, "Microstructure–Properties Relationship in a One-Step Quenched and Partitioned Steel," *Materials Science and Engineering A,* Vol. 589, 2014, pp. 101–111.
18. S. Yan and X. Liu, "Microstructure and Mechanical Properties of a Low-Carbon Steel Treated by One-Step Quenching and Partitioning Process," *Advanced Materials Research,* Vol. 1082, No. 1662–8985, 2015, pp. 202–207.
19. G.A. Thomas, J.G. Speer and D.K. Matlock, "Considerations in the Application of the 'Quenching and Partitioning' Concept to Hot-Rolled AHSS Production," *International Conference on New Developments in Advanced High-Strength Sheet Steels,* 2008, pp. 227–236.
20. Y. Xu, X. Tan, X. Yang, Z. Hu, F. Peng, D. Wu, G. Wang, D. Wu and G. Wang, "Microstructure Evolution and Mechanical Properties of a Hot-Rolled Directly Quenched and Partitioned Steel Containing Proeutectoid Ferrite," *Materials Science and Engineering A,* Vol. 607, 2014, pp. 460–475.
21. G. Thomas, "Simulation of Hot-Rolled Advanced High Strength Sheet Steel Production Using a Gleeble System," M.S. thesis, Colorado School of Mines, 2009.
22. S.C. Hong, J.C. Ahn, S.Y. Nam, S.J. Kim, H.C. Yang, J.G. Speer and D.K. Matlock, "Mechanical Properties of High-Si Plate Steel Produced by the Quenching and Partitioning Process," *Metals and Materials International,* Vol. 13, No. 6, 2007, pp. 439–445.
23. S. Zhou, K. Zhang, N. Chen, J. Gu and Y. Rong, "Investigation on High Strength Hot-Rolled Plates by Quenching-Partitioning-Tempering Process Suitable for Engineering," *ISIJ International,* Vol. 51, No. 10, 2011, pp. 1688–1695.
24. M.C. Somani, L.P. Karjalainen, D.A. Porter and D.K. Misra, "Evaluation of the Behavior and Properties of a High-Si Steel Processed Using Direct Quenching and Partitioning," *Materials Science Forum,* Vol. 706–709, 2012, pp. 2824–2829.
25. T.L. Bergman and A.S. Lavine, *Fundamentals of Heat and Mass Transfer,* 7th ed., John Wiley & Sons Inc., Hoboken, N.J., USA, 2011.
26. C.R. Brooks, "Principles of the Heat Treatment of Plain Carbon and Low-Alloy Steels," *Principles of the Heat Treatment of Plain-Carbon and Low-Alloy Steels,* ASM International, Materials Park, Ohio, USA, 1996, pp. 89–126.
27. H.M. Tensi, A. Stich and G.E. Totten, "Process Variables Affecting Cooling Behavior and Heat Transfer," *Steel Heat Treatment Handbook,* First Edit., G.E. Totten and M.A.H. Howes, eds., Marcel Dekker Inc., New York, N.Y., USA, 1997, pp. 185–197.
28. K. Okamoto, A. Yoshie and H. Nakao, "Physical Metallurgy of Direct Quenched Steel Plates and Its Application for Commercial Processes and Products," *Physical Metallurgy of Direct-Quenched Steels, Proceedings of TMS,* 1992, pp. 340–344.
29. Y. Meng and B.G. Thomas, "Heat Transfer and Solidification Model of Continuous Slab Casting: CON1D," *Metallurgical and Materials Transactions B,* Vol. 34, October 2006, pp. 685–705.
30. C. Li and B.G. Thomas, "Thermomechanical Finite-Element Model of Shell Behavior in Continuous Casting of Steel," *Metallurgical and Materials Transactions B,* Vol. 35 B, 2004, pp. 1151–1172.
31. V. Rudnev, D. Loveless, R. Cook and M. Black, "Induction Mass Heating," *Handbook of Induction Heating,* CRC Press, New York, N.Y., USA, 2003, pp. 623–625. ✦

AISTech This paper was presented at AISTech 2017 — The Iron & Steel Technology Conference and Exposition, Nashville, Tenn., USA, and published in the Conference Proceedings.